Journal of Computational Applied Mechanics 2024, 55 (-): PP-PP

DOI: 10.22059/JCAMECH.2024.371990.965

RESEARCH PAPER

Numerical Simulation of Laminar Flow of a Non-Newtonian Bentonite Solution in a Horizontal Pipe

Kherief Nacereddine Abdelhakim [a,*], Kholai Omar [a], Chekired Mourad [b], Kadja Mahfoud [b], Ton Hoang Mai [c]

[a] *Laboratoire Ingénierie des Transports et Environnement (LITE), Université Constantine 1, Constantine 25000, Algeria*

[b] *Laboratoire d'Energetique Appliquee et de Pollution, Faculté des Sciences de la Technologie, Université Frères Mentouri, Algeria*

[c] *Groupe de Recherche en Sciences pour l'Ingénieur, SFR Condorcet FR CNRS 3417, Université de Reims Champagne-Ardenne, France*

Abstract

The present study constitutes a notable contribution to enhancing our understanding of the behavior exhibited by non-Newtonian fluids. The purpose of the study involves conducting numerical simulations that elucidate the laminar flow dynamics within a horizontal pipe. The investigated flowing medium consists of bentonite suspensions with varying concentrations. The rheological behavior of the fluid is accurately described using the Herschel-Bulkley model, a pseudo-plastic representation. The results obtained through this research have helped to meticulously analyze the influence of fluctuations in the rheological index *n* on the following flow key parameters: pressure drop, velocity, and coefficient of friction within the pipe. This analysis covers a range of generalized Reynolds numbers, all the values of which correspond to the laminar flow regime. The meticulous study of the flow parameters reveals a compelling alignment between the simulation results and the experimental measurements, which underscores the validity of the study's findings.

Keywords: non-Newtonian fluid; Bentonite; numerical simulation; horizontal pipe; laminar flow.

1. Introduction

The study of non-Newtonian suspensions is considered to be one of the most common studies currently undertaken in fluid mechanics because of their extensive use in pipeline transport operations and in other important industrial fields (pharmaceutical, biological, petroleum, etc.).

The studies of non-Newtonian fluid dynamics which appeared in many articles published during the last decades focused on the hydrodynamic properties of these fluids, such as pressure drops in pipes [1]. For example [2] conducted this study in a non-circular pipe. Among these fluids, non-Newtonian suspensions and solutions stand out for their intricately complex rheological properties, making them the focal point of extensive study, as evidenced by research such as that conducted by [3, 4]. Many authors have published the results of their studies on these fluids [5-7]. Various mathematical models have been used for their modeling. Several experimental studies have also been conducted on these fluids, such as the studies on the bentonite solution which have been published by [8, 9].

In recent years, various researches consisted in the study of the dynamics of these materials in different flow regimes and the problem of transition to turbulence [10-12]; conducted studies related to the influence of the variation of the Reynolds number on the profile of the velocity in a pipe; also [13-16] analyzed numerically the hydrodynamic and thermal behaviors of these fluids as the flow behavior index *n* and the Reynolds number Re are varied; usually the increase or decrease in the flow behavior index *n* depends on the concentrations of suspensions added to non-Newtonian substances as was observed by [5, 7, 8, 17-20]. Given the challenging behavior of

* Corresponding author. *E-mail address:* Hakimkherief21@gmail.com

bentonite solutions, a significant number of researchers are presently directing their attention towards conducting a thorough investigation of the intermolecular, ionic, and electrical properties intrinsic to these non-Newtonian substances. This pursuit aims to enhance the comprehension of diverse phenomena associated with them across various domains. This trend is exemplified in the studies published by [21-25].

The present study aims to clarify the influence of the flow behavior index *n* in the viscosity equation and the Reynolds number on the variation of the velocity profile and the friction coefficient in a circular pipe. The effects of these two parameters on the shear stress at the inner wall of the pipe are also analyzed. This study has been achieved by increasing the concentration of bentonite in the dispersing solution (water) and by increasing the initial velocity that affects the Reynolds number. The obtained results have been compared with the experimental data published by [18].

2. Nomenclature

D	pipe diameter D=2R (m)
k	flow consistency index (Pa.s^n)
L	pipe length (m)
n	flow behavior index
r	radial coordinate (m)
R	dimensionless radius
Re_{MR}	Metzner and Reed generalized Reynolds number
U	dimensionless axial velocity
v	instantaneous velocity (m.s^{-1})
V	dimensionless radial velocity
V_m	initial velocity or average velocity at the entrance (m.s^{-1})
V_r	radial velocity component (m.s^{-1})
V_z	axial velocity component (m.s^{-1})
V_θ	azimuthal velocity component (m/s)
W	dimensionless angular velocity
z	axial coordinate (m)
Z	dimensionless axial length
Greek letters	
γ	shear rate(s^{-1})
θ	angular coordinate (m)
ρ	density (kg.m^{-3})
τ	shear stress (Pa)
τ_0	yield stress (Pa)
μ_{eff}	effective viscosity of the fluid (Pa. s)

3. Mathematical Model

From the experimental results obtained by [18] on the thixotropy of the fluid studied and the elasticity and viscous models of a bentonite suspension, we can consider that the mathematical formulation closest to the modeling is the Herschel Bulkley model:

$$\tau = \tau_0^H + k\dot{\gamma}^n \qquad for \qquad |\tau_{yx}| > |\tau_0^H| \tag{1}$$

$$\dot{\gamma} = 0 \qquad for \qquad |\tau_{yx}| < |\tau_0^H| \tag{2}$$

Where τ represents the shear stress, τ_0 the yield stress of the studied fluid, $\dot{\gamma}$ the flow shear rate, *n* is the flow behavior index of the fluid, and *k* is the flow consistency index.

Table 1 presents the rheological and physical characteristics of the used fluid (Bentonite solution at different concentrations); these results have been taken from the experimental studies of [18, 26].

Table 1: Rheological and physical properties for Bentonite solution at different concentrations

	n	***k***	**τ_0(Pa)**	**ρ(kg.m^{-3})**
Bentonite (8%)	0,59	0,57	10,58	1050
Bentonite (5%)	0,68	0,11	0,03	1030
Bentonite (3,5%)	0,79	0,03	0,02	1022

We consider the stationary and laminar flow (Re≤ 2100) of Herschel bulkley fluid inside a circular pipe of length

L and radius R such that the value of (L/R) is very large, see Fig. 1 and Fig. 2.

The mass and momentum conservation equations, which govern this flow, are as follows [27]

Continuity equation:

$$\frac{\partial \rho}{\partial t}+\frac{1}{r}\frac{\partial}{\partial r}(\rho r V_r)+\frac{1}{r}\frac{\partial}{\partial \theta}(\rho V_\theta)+\frac{\partial}{\partial z}(\rho V_z)=0 \tag{3}$$

Momentum equations: Momentum Equations in *r*, *θ*, and *z* directions, respectively:

In r direction:

$$\begin{aligned}\rho\left(\frac{\partial V_r}{\partial t}+V_r\frac{\partial V_r}{\partial r}+\frac{V_\theta}{r}\frac{\partial V_r}{\partial \theta}-\frac{V_\theta^2}{r}+V_z\frac{\partial V_r}{\partial z}\right)&\\ =-\frac{\partial p}{\partial r}&\\ +\left[\frac{1}{r}\frac{\partial}{\partial r}\left(\mu_{eff}r\frac{\partial V_r}{\partial r}\right)+\frac{1}{r^2}\frac{\partial}{\partial \theta}\left(\mu_{eff}\frac{\partial V_r}{\partial \theta}\right)+\frac{\partial}{\partial z}\left(\mu_{eff}\frac{\partial V_r}{\partial z}\right)-\frac{2\mu_{eff}}{r^2}\frac{\partial V_\theta}{\partial \theta}+\frac{V_r}{r}\frac{\partial \mu_{eff}}{\partial r}-\frac{\mu_{eff}V_r}{r^2}\right.&\\ \left.+\frac{\partial \mu_{eff}}{\partial z}\frac{\partial V_z}{\partial r}+\frac{\partial \mu_{eff}}{\partial \theta}\frac{\partial}{\partial r}\left(\frac{V_\theta}{r}\right)+r\frac{\partial \mu_{eff}}{\partial r}\frac{\partial}{\partial r}\left(\frac{V_r}{r}\right)\right]+\rho g_r&\end{aligned} \tag{4}$$

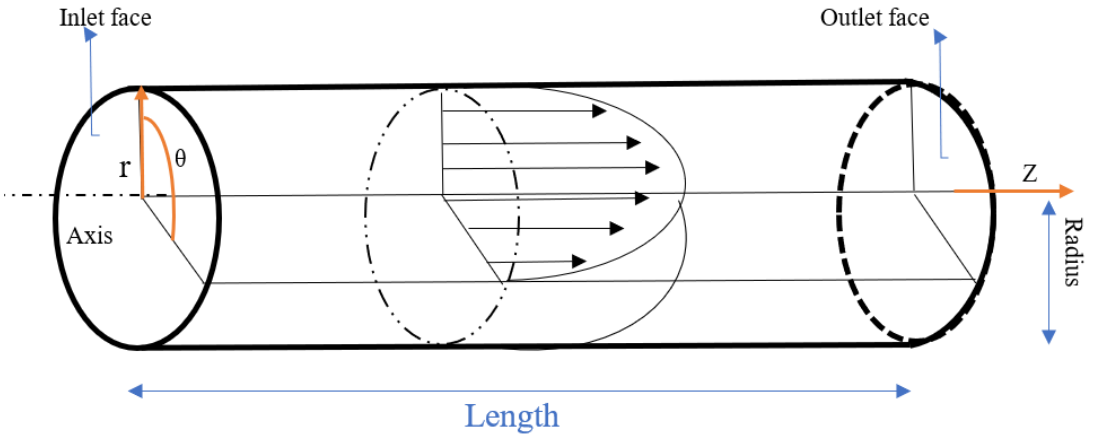

Fig. 1. Geometry and coordinate system of the pipe flow

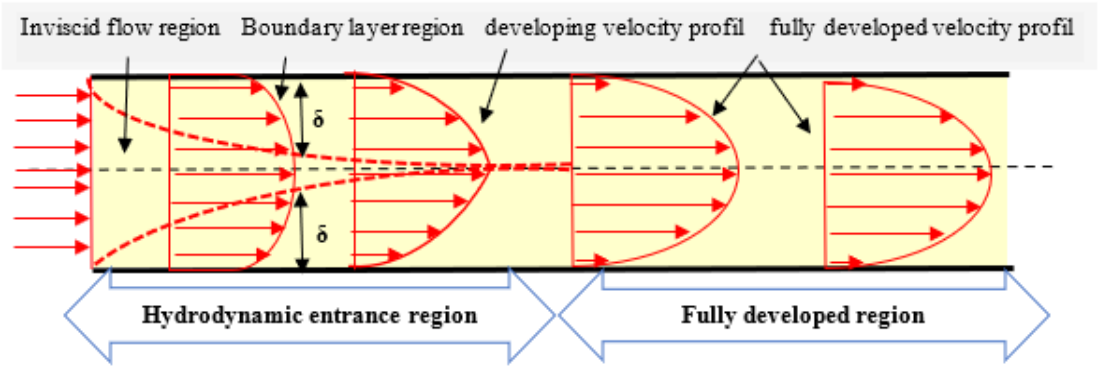

Fig. 2. schematic representation of the laminar pipe flow in the r-z plane

In θ direction:

$$\begin{aligned}\rho\left(\frac{\partial V_\theta}{\partial t}+V_r\frac{\partial V_\theta}{\partial r}+\frac{V_\theta}{r}\frac{\partial V_\theta}{\partial \theta}+\frac{V_\theta V_r}{r}+V_z\frac{\partial V_\theta}{\partial z}\right)=-\frac{1}{r}\frac{\partial p}{\partial \theta}+\left[\frac{1}{r}\frac{\partial}{\partial r}\left(\mu_{eff}r\frac{\partial V_\theta}{\partial r}\right)+\frac{1}{r^2}\frac{\partial}{\partial \theta}\left(\mu_{eff}\frac{\partial V_\theta}{\partial \theta}\right)+\frac{\partial}{\partial z}\left(\mu_{eff}\frac{\partial V_\theta}{\partial z}\right)+\right.&\\ \left.\frac{2\mu_{eff}}{r^2}\frac{\partial V_r}{\partial \theta}-\frac{\mu_{eff}V_\theta}{r^2}+\frac{1}{r}\frac{\partial \mu_{eff}}{\partial z}\frac{\partial V_z}{\partial \theta}+\frac{1}{r^2}\frac{\partial \mu_{eff}}{\partial \theta}\left(\frac{\partial V_\theta}{\partial \theta}+2V_r\right)+\frac{1}{r}\frac{\partial \mu_{eff}}{\partial r}\left(\frac{\partial V_r}{\partial \theta}-V_\theta\right)\right]+\rho g_\theta&\end{aligned} \tag{5}$$

In z direction:

$$\rho\left(\frac{\partial V_z}{\partial t}+V_r\frac{\partial V_z}{\partial r}+\frac{V_\theta}{r}\frac{\partial V_z}{\partial \theta}+V_z\frac{\partial V_z}{\partial z}\right)=-\frac{\partial p}{\partial r}+\left[\frac{1}{r}\frac{\partial}{\partial r}\left(\mu_{eff}\,r\frac{\partial V_z}{\partial r}\right)+\frac{1}{r^2}\frac{\partial}{\partial \theta}\left(\mu_{eff}\frac{\partial V_z}{\partial \theta}\right)+\frac{\partial}{\partial z}\left(\mu_{eff}\frac{\partial V_z}{\partial z}\right)+\frac{\partial \mu_{eff}}{\partial r}\frac{\partial V_r}{\partial z}+\frac{1}{r}\frac{\partial \mu_{eff}}{\partial \theta}\frac{\partial V_\theta}{\partial z}+\frac{\partial \mu_{eff}}{\partial z}\frac{\partial V_z}{\partial z}\right]+\rho g_z \tag{6}$$

Where:

- $V_r(r,\theta,z)$, $V_\theta(r,\theta,z)$, and $V_z(r,\theta,z)$ are the radial, azimuthal, and axial velocity components, respectively,
- $p(r,\theta,z)$ is the pressure,
- ρ is the density of the fluid,
- μ_{eff} denotes the effective viscosity of the Hershel-Bulkley fluid, expressed as [28]

$$\mu_{eff}=\frac{\tau_0}{\dot{\gamma}}+k(\dot{\gamma})^{n-1} \qquad for \qquad \tau \geq \tau_0 \tag{7}$$

$$\mu_{eff}=\infty \qquad for \qquad \tau \leq \tau_0 \tag{8}$$

The fluid is considered as incompressible with the assumption of a steady flow. The following boundary conditions are adopted:

- Stationary flow: $\frac{\partial}{\partial t}$
- Incompressible fluid: ρ=cte
- There is no rotation of the fluid in the pipe and the flow is axisymmetric flow: $\frac{\partial}{\partial \theta}$
- The boundary conditions:
  - ✓ At the entrance to the pipe:

$$\begin{cases}0\leq r\leq D/2\\ 0\leq\theta\leq\pi\\ z=0\end{cases} \qquad \begin{cases}V_r=V_\theta\\ V_z=V_0\end{cases} \tag{9a}$$

  - ✓ At the pipe wall:

$$\begin{cases}r=D/2\\ 0\leq\theta\leq\pi\\ 0\leq z\leq l\end{cases} \qquad V_r=V_\theta=V_z=0 \tag{10b}$$

  - ✓ At the exit of the pipe:

$$\begin{cases}0\leq r\leq D/2\\ 0\leq\theta\leq\pi\\ z=l\end{cases} \qquad \frac{\partial V_r}{\partial z}=\frac{\partial V_\theta}{\partial z}=\frac{\partial V_Z}{\partial z}=0 \tag{11c}$$

In order to extend and generalize the problem, the use of equations (3) to (6) in their dimensionless form is necessary. We
define the non-dimensional quantities, as follows

$$R=\frac{r}{D} \qquad Z=\frac{z}{L} \qquad U=\frac{V_z}{V_m} \qquad W=\frac{V_\theta}{V_m} \qquad V=\frac{V_r}{V_m} \qquad P^*=\frac{P}{\rho V_0^2}$$

By using these non-dimensional quantities, the conservation equations (3) to (6) , will then be written as follows

Dimensionless continuity equation:

$$\frac{1}{R}+\frac{\partial(RV)}{\partial R}+\frac{\partial U}{\partial Z}=0 \tag{12}$$

Dimensionless momentum equations
radial direction (direction R)

$$\frac{1}{\mathrm{R}}+\frac{\partial(RVV)}{\partial R}+\frac{\partial(UV)}{\partial Z}=-\frac{\partial P^{*}}{\partial Z}+\frac{1}{\mathrm{Re}}\left[\frac{1}{\mathrm{R}}\frac{\partial}{\partial R}\left(\mu_{eff}\mathrm{R}\frac{\partial U}{\partial R}\right)+\frac{\partial}{\partial Z}\left(\mu_{eff}\frac{\partial U}{\partial Z}\right)\right]+\frac{1}{\mathrm{Re}}\left[\frac{1}{\mathrm{R}}\frac{\partial\mu_{eff}}{\partial R}-\mu_{eff}\frac{\mathrm{V}}{\mathrm{R}^{2}}+\frac{\partial\mu_{eff}}{\partial Z}\frac{\partial U}{\partial R}+\mathrm{R}\frac{\partial\mu_{eff}}{\partial R}\frac{\partial}{\partial R}\left(\frac{\mathrm{V}}{\mathrm{R}}\right)\right] \quad (13)$$

Axial direction (direction Z)

$$\frac{1}{\mathrm{R}}+\frac{\partial(RVU)}{\partial R}+\frac{\partial(UU)}{\partial Z}=-\frac{\partial P^{*}}{\partial Z}+\frac{1}{\mathrm{Re}}\left[\frac{1}{\mathrm{R}}\frac{\partial}{\partial R}\left(\mu_{eff}\mathrm{R}\frac{\partial U}{\partial R}\right)+\frac{\partial}{\partial Z}\left(\mu_{eff}\frac{\partial U}{\partial Z}\right)\right]+\frac{1}{\mathrm{Re}}\left[\frac{\partial\mu_{eff}}{\partial R}\frac{\partial V}{\partial Z}+\frac{\partial\mu_{eff}}{\partial Z}\frac{\partial U}{\partial Z}\right] \quad (14)$$

The momentum equation in the θ direction can be neglected from the hypothesis of axisymmetric flow, for this reason we find only the equation on the axial and radial direction.

Now the boundary conditions for the dimensionless equations of continuity and momentum as fellow:

✓ At the entrance to the pipe

$$\begin{cases}0\le R\le 0.5\\ \quad and\\ \quad z=0\end{cases}\qquad \begin{cases}\mathrm{V}=0\\ \mathrm{U}=1\end{cases} \quad (15a)$$

✓ At the pipe wall:

$$\begin{cases}R=0{,}5\\ \quad and\\ 0\le Z\le L\end{cases}\qquad U=V=0 \quad (16b)$$

✓ At the exit of the pipe:

$$\begin{cases}0\le R\le 0.5\\ \quad \text{and}\\ \quad Z=L\end{cases}\qquad \frac{\partial \mathrm{V}}{\partial Z}=\frac{\partial \mathrm{U}}{\partial Z}=0 \quad (17c)$$

From the equation provided (11) and (12), the Reynolds number (Re) can be determined as follows:

$$\mathrm{Re}=\frac{\rho \mathrm{V}_{0}^{2}\mathrm{D}}{\mu_{eff}} \quad (18)$$

In general, for non-Newtonian liquids the effective viscosity is used for calculation and defined [28]

$$\mu_{eff}=k'\left(\frac{8V}{D}\right)^{n'-1} \quad (19)$$

When: $k'=k\frac{3n'+1}{4n'}$ and $n'=n$ for some the models of power low and Herschel- Bulkley.

Substituting into equation (12) we find:

$$\mathrm{Re}=\frac{\rho D^{n}V^{2-n}}{k\left(\frac{3n+1}{4n}\right)^{n}*8^{n-1}} \quad (20)$$

Here, Re represents a generalized Reynolds number ($\mathrm{Re_{MR}}$) valid for all time-independent non-Newtonian fluids represents by Metzner et Reed [29].

4. Numerical methods:

4.1. Grid generation

Achieving accurate numerical results requires the creation of suitable meshes for the numerical simulation using Ansys fluent. This is confirmed by a number of authors, such as [30] who presented a study on the improvement of the characteristics of the geometric meshing by improving the quality of the mesh at the boundaries. Also, the researchers [31] conducted studies to compare the efficiency of the finite volume method with that of finite elements method using various simulation meshes. On the other hand, some researchers [32-35] investigated the properties of mesh modification based on the node and element, and concluded that the numerical modeling is closely related to the shape of mesh used, and that the shape of quadratic element mesh gives better results than the shape of triangular element for numerical modeling of flow through a cylinder, whether in two or in three dimensions.

In order to reach the best precision of the numerical solution in the present study, we chose the mesh after three trials using three different types of mesh. Different features characterize each mesh, for the same dimensions and geometric shape of the three-dimensional cylinder. Table 2 summarizes the most important differences in the meshes.

Table 2 Characteristics of the three tried mesh types

Cases / Differences	Case 01	Case 02	Case 03
Free face mesh type	Single quadrilateral	Single quadrilateral	Single quadrilateral
mesh type	Non uniform	uniform	Non uniform
Nodes Number in the boundary layer	20	/	20
rate of growth	1.2	1.	1.2
Number of nodes	484484	100793	352772
Number of volumes	473000	96120	345900

The simulation results are presented in Fig. 3 and compared with the measurements of [18]. It can be observed that the accuracy of the simulation process is closely related to the mesh, and that the rise of the number of cells and nodes plays an important role in improving the precision of the numerical results, especially at the region near the walls of the cylinder for both the velocity profile and pressure drop, especially with viscous materials.

The best results in these three trials are obtained with the type 1 mesh. Hence, it is adopted for all the simulation processes in this study. The mesh is presented in Fig. 4.

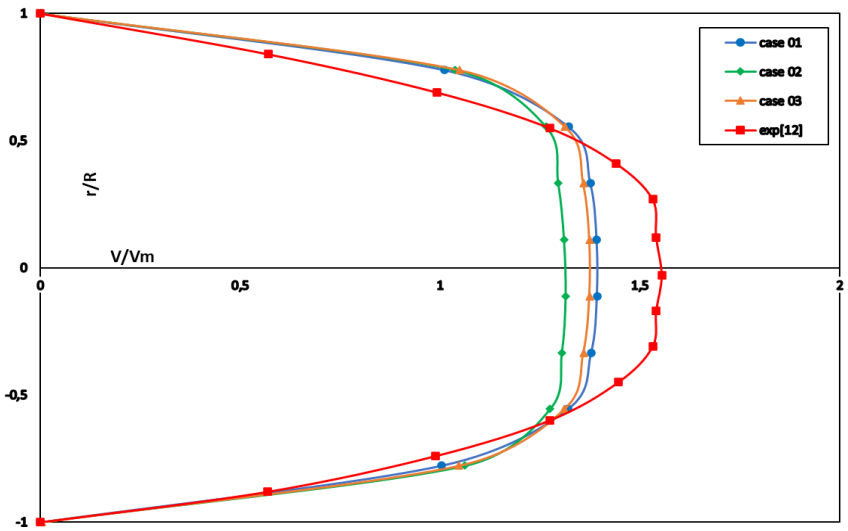

Fig. 3.Dependence of the numerical modeling results on mesh type

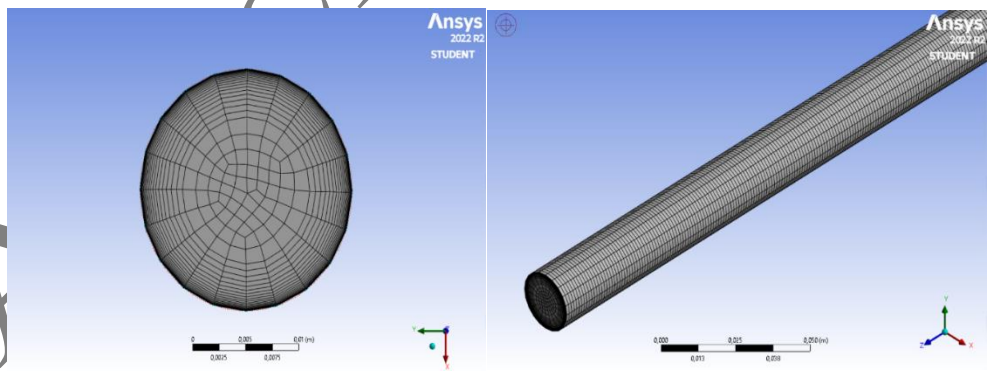

Fig. 4. Illustration of the geometry and mesh used

4.2. Solution of the governing equations

The calculations were done using the commercial CFD code "ANSYS FLUENT version R2 2022". The finite volume method is used in this code to discretize the governing partial differential equations. The second order upwind differencing scheme is used for the formulation of the convection-diffusion contribution to the coefficients in the finite-volume equations. The discretization yields a set of linear algebraic equations for the velocity components and the pressure. A pressure-velocity coupling algorithm is then used to solve iteratively this set of algebraic equations. This coupling was chosen among the three pressure-velocity coupling algorithms available in ANSYS (SIMPLE, SIMPLER and Coupled). Previous studies on these couplings [36, 37] have shown a small difference in the convergence of the solutions, in addition to the speed and time of the simulation processes.

The results of the simulations achieved with each of these couplings are shown in Fig. 5. One can notice that the results of numerical modeling using the Coupled algorithm are the closest to the experimental results. As a consequence, this method was chosen to perform all the simulations reported in the present study. The algorithm is presented in the Appendix.

The convergence criteria for terminating the iterations of all the numerical simulations performed in this study are based on the normalized residuals for each governing equation. The computations are stopped when the scaled residuals for the continuity and momentum equations reach values below 10^{-5}. Once these computations are completed, the results obtained are analyzed with the post-processing capability embedded in the code.

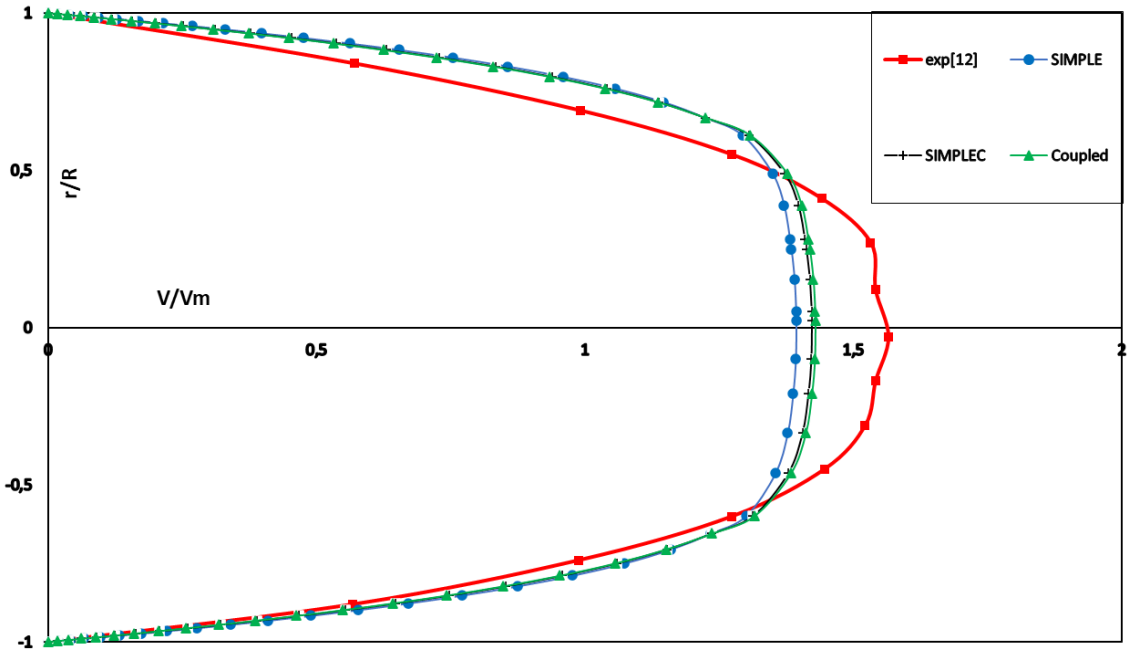

Fig. 5. Comparison of the numerical modeling results obtained using different pressure velocity coupling algorithms with the measurements of Benslimane et al [12]

5. Results and discussions:

The results obtained throughout this research are presented graphically in figures 5-11.

5.1. *Effect of the index n*

First, we studied the effect of the index n on the flow of the fluid inside the pipe. We took into account the three fluids with different concentrations of bentonite and modeled them using the rheological and physical properties shown in Table 1. We also simulated the flow of the pure base fluid i.e. water, which is a Newtonian fluid, in order to understand the effect of the non-Newtonian behavior well. The computational results obtained for bentonite solution flow inside the cylinder were compared with the experimental results of the study performed by [18] in the laminar regime. This comparison was achieved by computing the relative error (or the percentage error) between the numerical values and the experimental data. The error is defined as:

$$\%\text{Error}=\frac{[X]_n-[X]_e}{[X]_n}*100 \quad (21)$$

Where $[X]_n$ is the value of numerical modeling and $[X]_e$ is the value of experimental study.

5.1.1. Velocity profile

Fig. 6 represents the velocity profile at the exit of the duct for the three bentonite solutions and also for the base fluid water. The results show that as the concentration of bentonite increases, the fluid becomes more viscous, exhibits more pronounced shear-thinning behavior and forms a plug zone in the region around the axis of the cylinder. This is due to the rheological properties of these fluids, which are evident in the reduction of the *n* index value with the augmentation of bentonite concentration. These observations are in accord with the mathematical relations and equations of the Poiseuille flow of a Hershel Bulkley fluid given in the studies of Chhabra and Richardson [27].

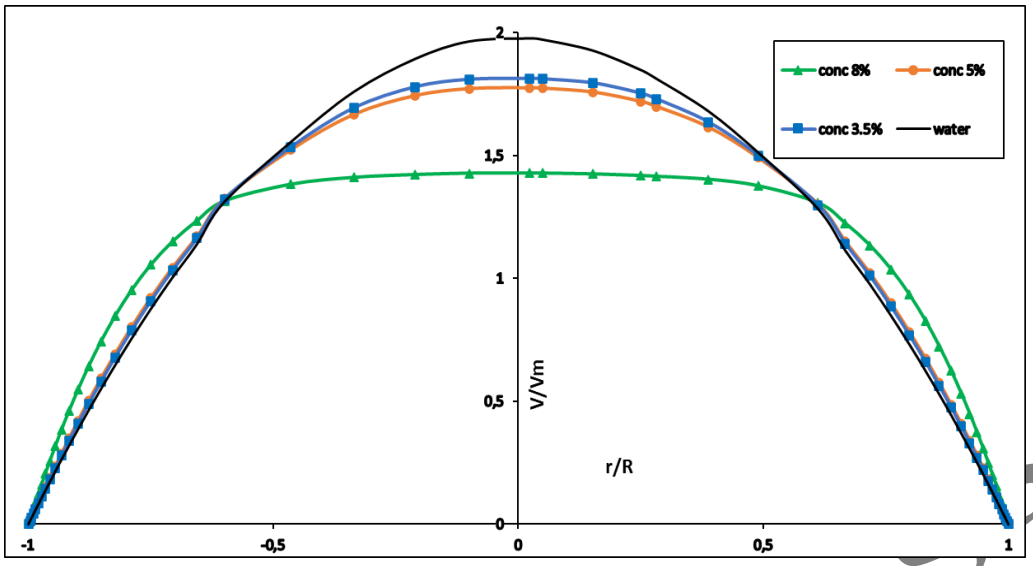

Fig. 6. Mean axial laminar velocity profiles for the three bentonite solutions and water

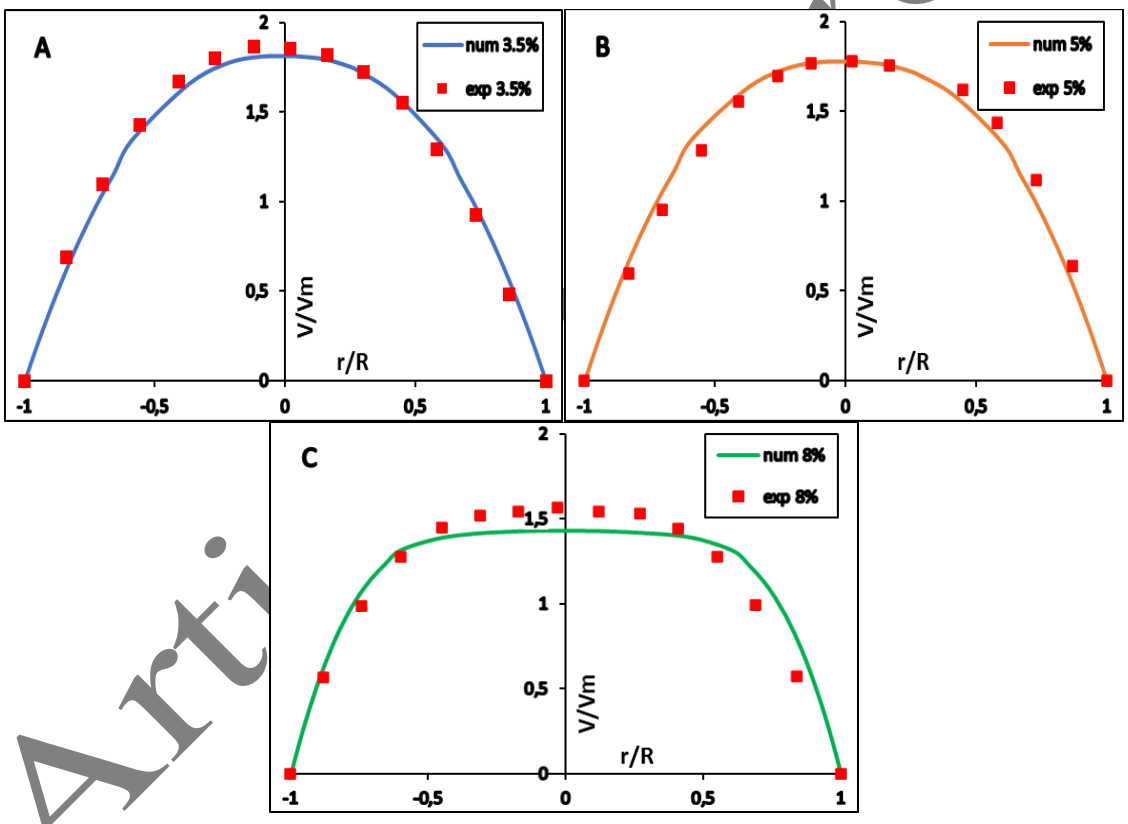

Fig. 7. Comparison of the numerical and experimental dimensionless velocity profiles for the three values of the index n, A: n=0.79, B: n=0.68 and C: n=0.59

Fig. 7 shows the comparison between the present numerical studies and Benslimane et al's experimental data [12]. The numerical results are very close to the experimental data, especially for low-concentration bentonite solutions. In the case of 3.5% and 5% concentration bentonite the percentage error varies in the interval ±2% to ±3%, while it reaches up to ±7% for the 8% concentration bentonite. The discrepancy in the value of the error is due to the complex rheological characteristics, from the increase in the yield stress τ_0 to the augmentation of the volumetric mass value of liquid, which leads to an imbalance in the results of fluid modeling inside the pipe. Moreover, as the concentration rises, intricate particle interactions become more pronounced, leading to aggregation and complex structural formations. These interactions give rise to non-linear rheological behaviors, including shear-thinning and yield stress, which significantly affect flow properties.

For a more understanding of the characteristics and effects resulting from varying concentrations of bentonite and the index *n*, an in-depth investigation was conducted. The study focused on examining the pressure drop along the length of the cylinder. Additionally, an analysis of the pressure distribution between the center and inner wall of the cylinder was carried out at both the inlet and outlet sections. The results presented in the following subsection

support and corroborate these observations, providing valuable insights into the intricate relationship between material properties, pressure variations, and mechanical conditions within the cylinders.

5.1.2. Pressure

Table 3 presents the values of the total pressure drop at the level of the inner wall of the cylinder along the pipe. We can notice an increase in the total drop values with an increase in the concentration of bentonite and a decrease in the index n. These results can also reinforce and justify the reason for the appearance of the velocity profile being flatter at high values of bentonite concentration. This increase can be attributed to the fact that at higher concentrations of bentonite in the mixture, the particles are more densely packed within the fluid. This dense packing increases the effective viscosity of the mixture. Viscosity can be thought of as the fluid's resistance to flow. When the viscosity is higher due to the densely packed particles, the fluid encounters greater resistance as it travels through the pipe. This increased resistance translates into a higher pressure drop along the length of the pipe. Additionally, the increase in pressure drop may be explained by the interaction between particles. At higher concentrations their interaction can create a "hindered flow" effect. These fine particles have a tendency to stick together or hinder each other's movement, effectively impeding the smooth flow of the fluid. This hindrance further contributes to the increased pressure drop observed in high-concentration bentonite-water mixtures.

Table 3 Pressure drop along a pipe for bentonite fluids of various concentrations

Pressure drop / concentration	ΔP(Pa)
Newtonian Fluid (water 0% bentonite concentration)	0.532112
solution 3.5% bentonite concentration	123.061
solution 5% bentonite concentration	514.315
solution 8% bentonite concentration	6111.447

In contrast, when the concentration of bentonite in the mixture decreases, the particles are more spread out within the fluid. This results in reduced particle-particle interactions and a lower effective viscosity. As a result, the fluid encounters less resistance to flow, leading to a lower pressure drop along the pipe.

In order to further understand this, we studied the transverse dynamic pressure distribution between the axis of the cylinder and the inner wall at the inlet and outlet of the pipe. The results are presented in Fig. 8 A and B.

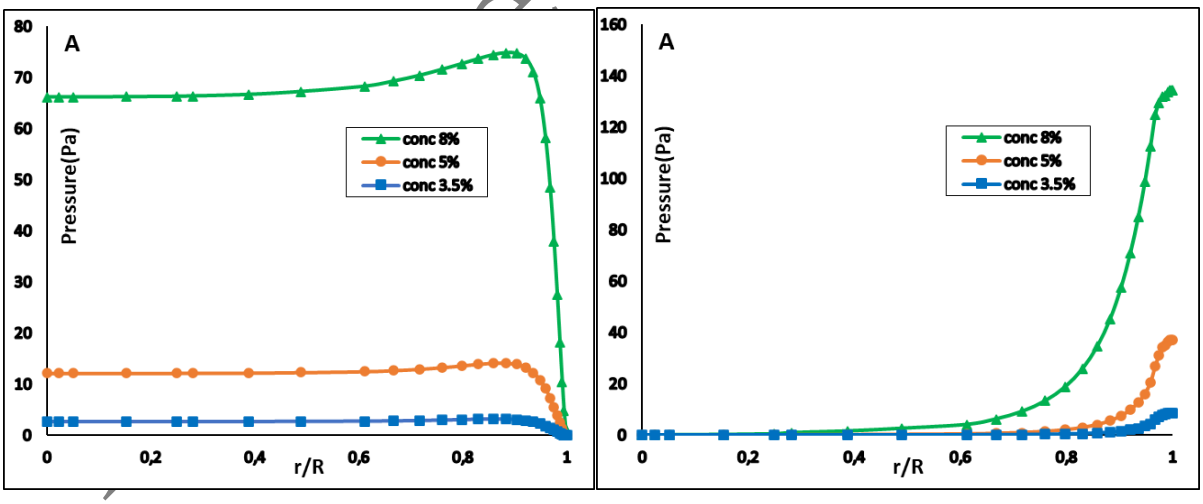

Fig. 8.The pressure distribution within the pipe, A) inlet section, B) outlet section

One can observe in Fig. 8A which corresponds to the inlet section that the pressure distribution within the cylindrical pipe is such that it is concentrated in the center of the entrance and that it is almost non-existent near the wall. However, Fig. 8B which corresponds to the outlet section shows a reversed pattern. This difference in pressure distribution between the inlet and outlet sections demonstrates the fascinating relationship between the concentration of bentonite in the non-Newtonian fluid and the resulting pressure differences.

The increase in pressure difference with an increase in the concentration of bentonite can be explained by the influence of the concentration on the rheological behavior of the non-Newtonian fluid. Bentonite is a common rheology modifier used to alter the flow properties of fluids. When bentonite is added to the non-Newtonian fluid, it affects the fluid's viscosity and shear-thinning/thickening behavior.

During the entrance phase, with low bentonite concentration, the fluid exhibits shear-thinning behavior. As the fluid accelerates towards the center of the cylinder, the shear rate in that region increases, leading to a decrease in viscosity. The lower viscosity near the center results in a decrease in pressure according to the Hagen-Poiseuille

equation and the Bernoulli principle. Therefore, the pressure is concentrated in the center of the cylinder.

As the concentration of bentonite increases, the shear-thinning behavior becomes more pronounced. The fluid's viscosity reduces significantly, leading to a more substantial decrease in pressure near the center during the entrance phase. Consequently, the pressure difference between the center and the wall increases as the concentration of bentonite increases.

At the outlet of the cylinder, the shear-thickening behavior dominates in the fluid. As the fluid exits the cylinder and its velocity decreases, the shear rate near the walls reduces, leading to an increase in viscosity. This increase in viscosity in the vicinity of the walls results in a rise in pressure along the walls and its diminishing towards the center.

Now, for an in-depth study of the movement of bentonite solution inside the cylinder, we have studied the behavior of this material for different values of the Reynolds numbers, which fall in the laminar flow range. also due to the fact that the non-Newtonian fluid at a high concentration of bentonite is very complex, and that its rheological properties and behaviors inside the pipe remain unstable, we preferred to take the lowest concentration values because they exhibit close similarity in rheological properties and yield stress values throughout the entire flow domain.

The obtained results have been compared with the experimental data of [18] and gave very close values for the velocity profile at the exit of the pipe.

5.2. Effect of the Reynolds number

5.2.1. Velocity

Fig. 9 and Fig. **10** show the evolution of the velocity profile as a function of Reynolds number for the two Bentonite solutions (n = 0.79) and (n = 0.68), respectively. There is a good agreement with the experimental results of [18] in the low Reynolds numbers range Re=360-620; also, for the large Reynolds numbers, which approach the transient regime Re values, one has a good agreement in the area close to the walls and a notable variation in the plug zone or the zone close to the axis. As Reynolds number increases, disturbances in the flow become more significant. The velocity profile in the axis region might start to deviate from the parabolic profile due to the complex interactions between viscosity changes and flow disturbances. These disturbances can cause fluctuations in velocity across the pipe diameter, which requires changing the measurement angle in more than one azimuthal position to extract a correct velocity profile. These profile defects have been noticed in similar experimental studies of the transition to turbulence for a non-Newtonian fluid by [10-12].

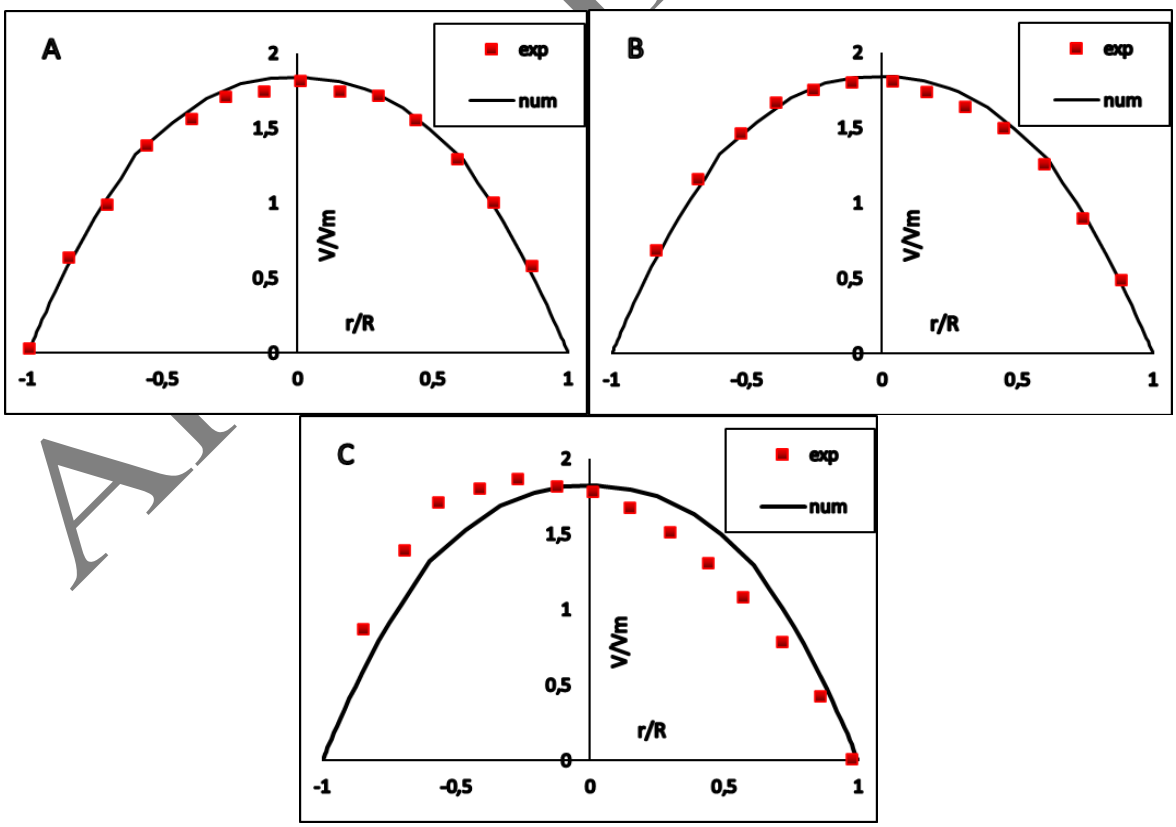

Fig. 9. Variation of dimensionless velocity profile through the radial position of bentonite solution n=0.79 for different Reynolds numbers: A)420, B)520, C)1350

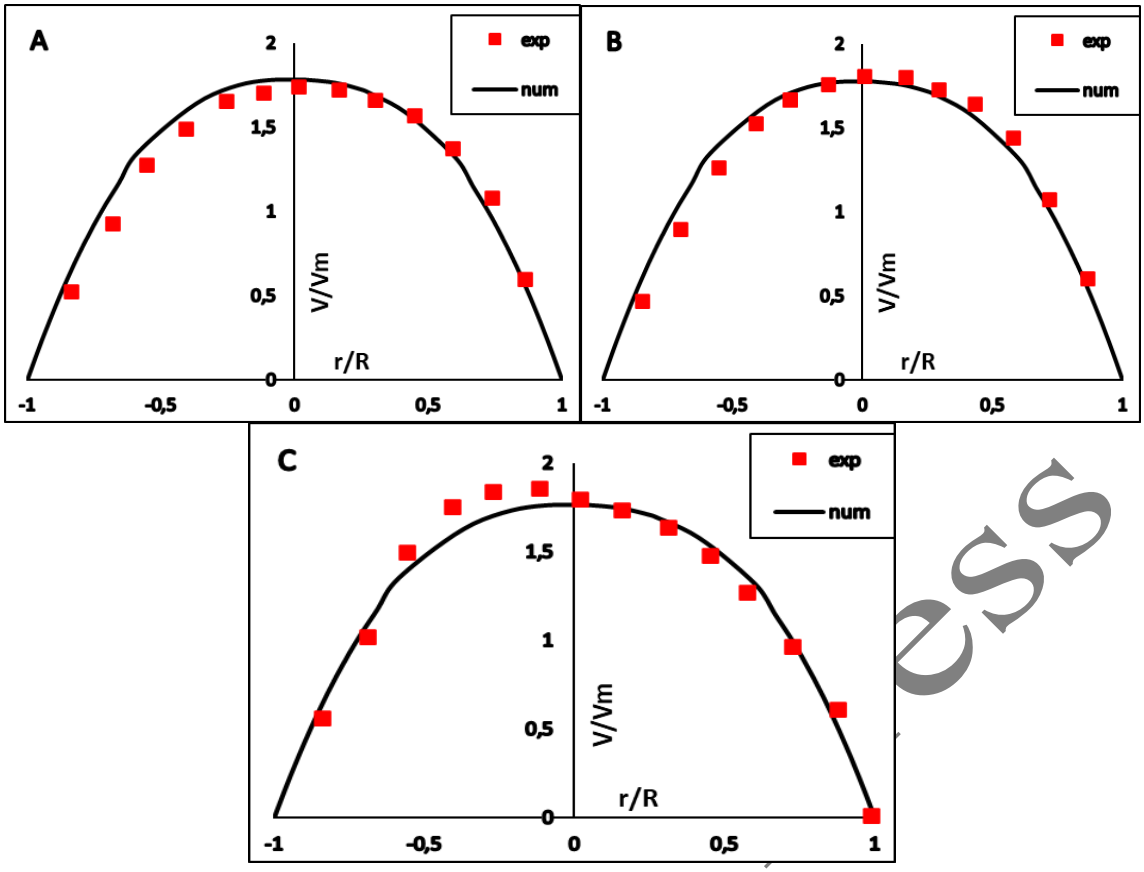

Fig. 10. Variation of dimensionless velocity profile through the radial position of bentonite solution n=0.68 for different Reynolds numbers: A)360, B)620, C)1150

In a normal Newtonian fluid flow, as the Reynolds number approaches its flow transition value, small turbulent eddies begin to form in the near-wall region. These eddies enhance mixing and disrupt the stagnant boundary layer. The presence of the non-Newtonian behavior, like shear-thinning, can complicate even more the near-wall velocity profile by affecting the effective viscosity and the resistance to flow at the wall. This can be seen clearly in the increasing pressure drop on the inner wall of both fluids, which is shown in Fig. 11.

5.2.2. Pressure

Fig. 11 represents the pressure drop value at the level of the wall between the inlet and outlet of the cylinder at different Reynolds numbers. As we can see, increasing the concentration of bentonite leads to an increase in pressure drop. This can be explained by the fact that the Reynolds number increase enhances the combined effects of heightened viscosity and the non-Newtonian behavior of the solution. For a given Reynolds number, higher bentonite concentrations result in increased viscosity, generating greater resistance to flow. Moreover, the non-Newtonian nature of bentonite solutions complicates their flow behavior, with viscosity changing with flow rate. For a given concentration, as the Reynolds number rises, the transition from laminar to turbulent flow amplifies fluid mixing and interaction, therefore intensifying pressure drop.

5.2.3. Friction factor

The evolution of the friction factor f as a function of Re_{MR} is presented in Fig. 12.
One can notice that there is a perfect agreement of the friction factor values at a low concentration of 3.5% of bentonite solution with the correlation of Fanning friction factor:

$$f = \frac{16}{Re_{MR}} \tag{22}$$

However, the values of the friction factor which correspond to the higher concentration of 5% are proportional to $10^{-1} f$. This can likely be attributed to the intricate interplay between viscosity changes and flow behavior. The higher concentration of bentonite at 5% could lead to stronger particle interactions and a more pronounced shear-thinning effect, causing a decrease in the effective viscosity as the flow rate increases. This reduction in viscosity at 5% concentration might result in a more streamlined flow with lower resistance to motion, consequently leading to a lower friction factor compared to the 3.5% concentration, where the viscosity might exhibit a different behavior under similar conditions.

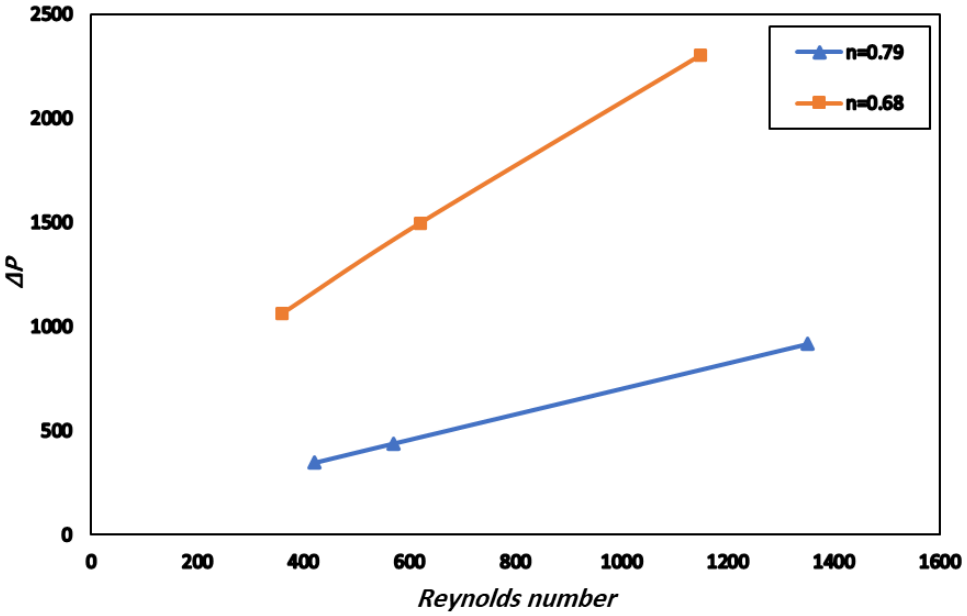

Fig. 11. Variation of pressure drops of the bentonite solutions as a function of the Reynolds number

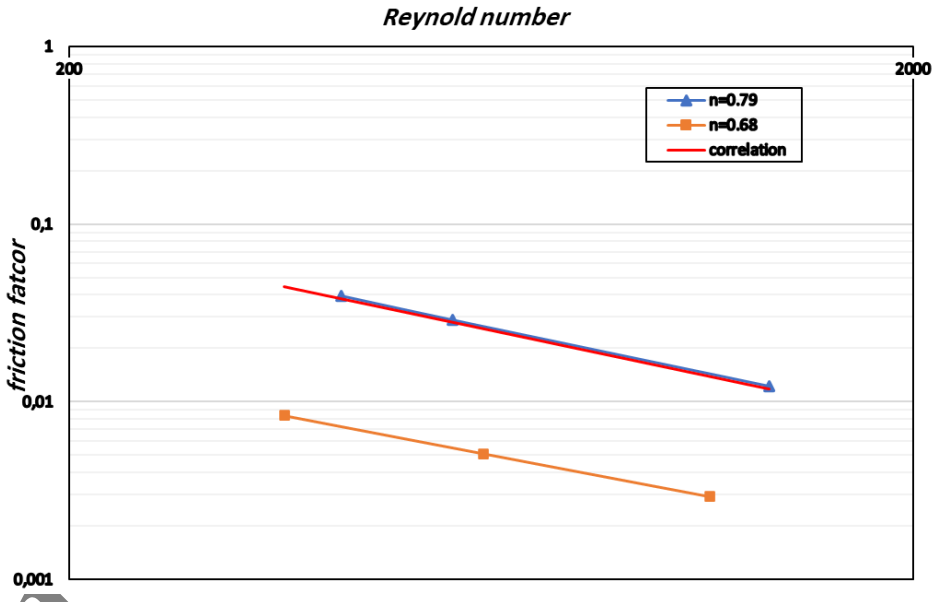

Fig. 12. Comparison of the coefficient of friction of bentonite solutions with the Fanning friction factor correlation

6. Conclusion

To conclude, the numerical investigation conducted on bentonite solutions spanning different concentrations has provided a profound understanding of the intricate behaviors exhibited by these fluids. The examination, centered around crucial factors such as velocity profiles, Reynolds numbers in laminar flow, pressure drop, and friction factors, has unveiled the nuanced connections between fluid concentration, flow characteristics, and fluid properties. The study's outcomes have showcased the pivotal role played by bentonite concentration in altering viscosity and evoking non-Newtonian traits, subsequently influencing velocity profiles. The exploration of Reynolds numbers within the laminar flow domain has unraveled insights into the underlying flow dynamics and their consequences. Additionally, the research has laid bare a direct relationship between concentration and pressure drops, illustrating that heightened concentrations lead to amplified pressure losses attributable to escalated viscosity and flow resistance. The examination of friction factors has further underscored the intricate interplay between flow conditions and fluid attributes. On the whole, this comprehensive inquiry establishes a bedrock for refining the transportation and manipulation of bentonite solutions across a spectrum of real-world applications, thereby enriching our comprehension of the behavior of non-Newtonian fluids.

Appendix A. Ansys fluent process

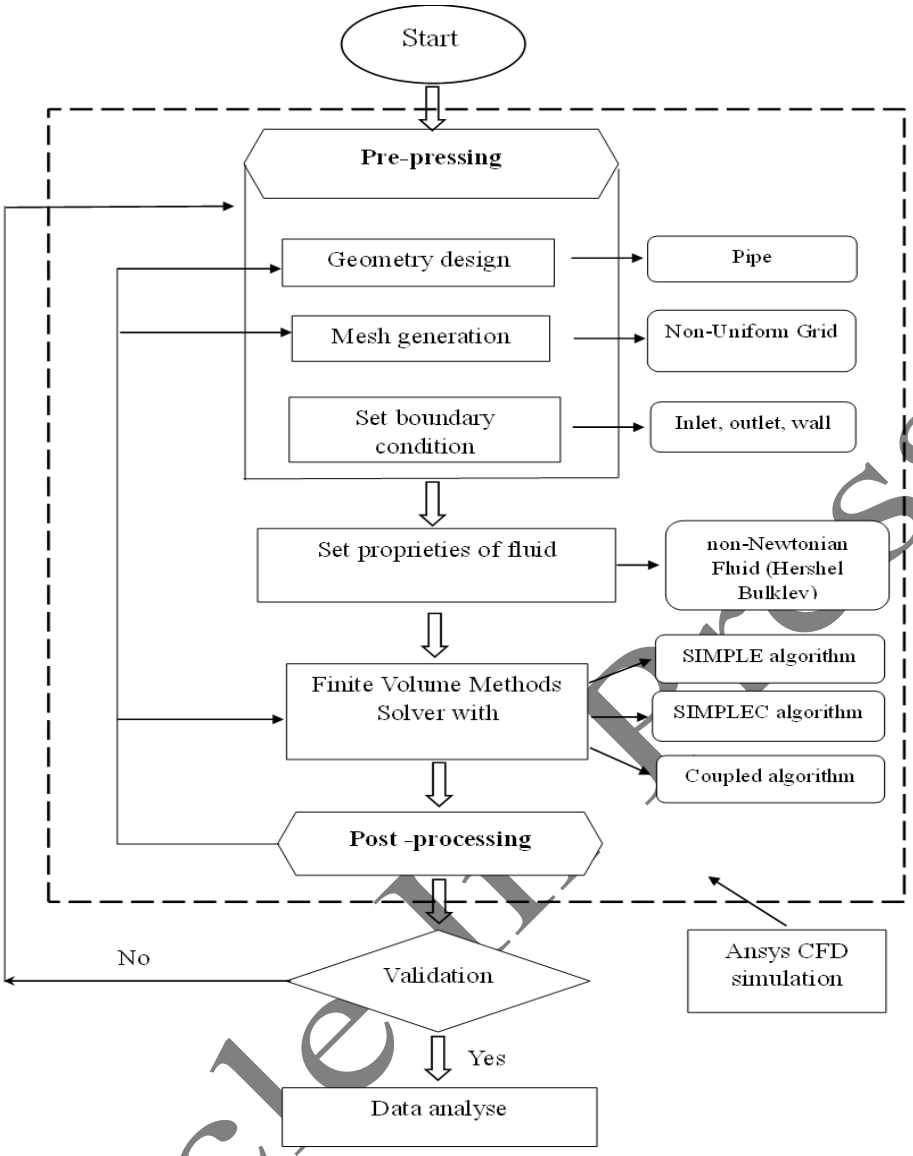

References

[1] B. Le Fur, M. Martin, Rapport I. a-3. Transport en conduite de liquides non-newtoniens, *Journées de l'hydraulique*, Vol. 9, No. 1, pp. 1-7, 1967.

[2] M. Mahfoud, S. Benhadid, M. Lebouché, Frottements et pertes de pression des fluides non newtoniens dans des conduites non circulaires, *Comptes Rendus Mécanique*, Vol. 333, No. 6, pp. 513-520, 2005.

[3] A. O. Ali, S. A. Khamis, F. S. Seif, O. D. Makinde, Entropy analysis of the unsteady Darcian nanofluid flow in a cylindrical pipe with a porous wall, *International Journal of Ambient Energy*, Vol. 43, No. 1, pp. 7321-7329, 2022.

[4] T. Chinyoka, O. Makinde, Viscoelastic modeling of the diffusion of polymeric pollutants injected into a pipe flow, *Acta Mechanica Sinica*, Vol. 29, pp. 166-178, 2013.

[5] U. Cartalos, P. Baylocq, J. Lecourtier, J. Piau, Caractérisation rhéologique et modélisation structurelle des systèmes argile-polymère. Application aux fluides de forage, *Revue de l'institut Français du Pétrole*, Vol. 52, No. 3, pp. 285-297, 1997.

[6] M. Naimi, R. Devienne, M. Lebouché, Etude dynamique et thermique de l'écoulement de Couette-Taylor-Poiseuille; cas d'un fluide présentant un seuil d'écoulement, *International journal of heat and mass transfer*, Vol. 33, No. 2, pp. 381-391, 1990.

[7] B. Fagla, M. Gradeck, C. Baravian, M. Lebouché, Étude expérimentale de l'hydrodynamique des suspensions non-newtoniennes de «grosses» particules dans une conduite horizontale, *Annales des Sciences Agronomiques*, Vol. 15, No. 1, 2011.

[8] S. Paumier, *FACTEURS DETERMINANT L'ORGANISATION ET LA RHEOLOGIE DU SYSTEME ARGILE-EAU POUR DES SUSPENSIONS DE SMECTITES*, Thesis, Ecole Supérieure d'Ingénieurs de Poitiers, 2007.

[9] K. Benyounes, A. Benchabane, A. Mellak, Caractérisation rhéologique de la bentonite de maghnia en suspension aqueuse sans et avec additifs anioniques, 2010.

[10] S. Gnambode, *Simulation des grandes échelles des transferts thermo-convectifs dans les écoulements turbulents d'un fluide non-newtonien en conduite cylindrique*, Thesis, Paris Est, 2015.

[11] S. N. López-Carranza, M. Jenny, C. Nouar, Pipe flow of shear-thinning fluids, *Comptes Rendus Mécanique*, Vol. 340, No. 8, pp. 602-618, 2012.

[12] N. Roland, *Modélisation de la transition vers la turbulence d'écoulements en tuyau de fluides rhéofluidifiants par calcul numérique d'ondes non linéaires*, Thesis, Institut National Polytechnique de Lorraine, 2010.

[13] O. D. Makinde, Analysis of non-Newtonian reactive flow in a cylindrical pipe, 2009.

[14] T. Chinyoka, O. D. Makinde, Computational dynamics of unsteady flow of a variable viscosity reactive fluid in a porous pipe, *Mechanics Research Communications*, Vol. 37, No. 3, pp. 347-353, 2010.

[15] N. T. Tayeb, S. Hossain, A. H. Khan, T. Mostefa, K.-Y. Kim, Evaluation of hydrodynamic and thermal behaviour of non-newtonian-nanofluid mixing in a chaotic micromixer, *Micromachines*, Vol. 13, No. 6, pp. 933, 2022.

[16] Y. Noori, A. R. Teymourtash, B. Zafarmand, Use of random vortex method in simulating non-newtonian fluid flow in a t-junction for various reynolds numbers and power-law indexes, *International Journal of Engineering*, Vol. 35, No. 5, pp. 954-966, 2022.

[17] T. Chinyoka, O. Makinde, On transient flow of a reactive variable viscosity third-grade fluid through a cylindrical pipe with convective cooling, *Meccanica*, Vol. 47, pp. 667-685, 2012.

[18] A. Benslimane, K. Bekkour, P. François, H. Bechir, Laminar and turbulent pipe flow of bentonite suspensions, *Journal of Petroleum Science and Engineering*, Vol. 139, pp. 85-93, 2016.

[19] Z. Wang, W. Guo, W. Ding, K. Liu, W. Qin, C. Wang, Z. Wang, Numerical study on the hydrodynamic properties of bentonite slurries with Herschel-Bulkley-Papanastasiou rheology model, *Powder Technology*, Vol. 419, pp. 118375, 2023.

[20] A. Abou-Kassem, M. Bizhani, E. Kuru, A review of methods used for rheological characterization of yield-power-law (YPL) fluids and their impact on the assessment of frictional pressure loss in pipe flow, *Geoenergy Science and Engineering*, pp. 212050, 2023.

[21] R. Deng, B. Chen, C. Liu, Concentration dependence of yield stress of bentonite suspension and corresponding particle interactions, *Computers and Geotechnics*, Vol. 157, pp. 105358, 2023.

[22] D. I. Al-Risheq, S. M. Shaikh, M. S. Nasser, F. Almomani, I. A. Hussein, M. K. Hassan, Enhancing the flocculation of stable bentonite suspension using hybrid system of polyelectrolytes and NADES, *Colloids and Surfaces A: Physicochemical and Engineering Aspects*, Vol. 638, pp. 128305, 2022.

[23] X. Li, Selective flocculation performance of amphiphilic quaternary ammonium salt in kaolin and bentonite suspensions, *Colloids and Surfaces A: Physicochemical and Engineering Aspects*, Vol. 636, pp. 128140, 2022.

[24] Z. Deng, X. Liu, X. Zhou, Q. Yang, P. Chen, A. de la Fuente, L. Ren, L. Du, Y. Han, F. Xiong, Main engineering problems and countermeasures in ultra-long-distance rock pipe jacking project: Water pipeline case study in Chongqing, *Tunnelling and Underground Space Technology*, Vol. 123, pp. 104420, 2022.

[25] H. Zhong, Y. Guan, Z. Qiu, B. P. Grady, J. Su, W. Huang, Application of carbon coated bentonite composite as an ultra-high temperature filtration reducer in water-based drilling fluid, *Journal of Molecular Liquids*, Vol. 375, pp. 121360, 2023.

[26] J. H. Burger, *Non-Newtonian open channel flow: the effect of shape*, Thesis, Cape Peninsula University of Technology, 2014.

[27] R. P. Chhabra, J. F. Richardson, 2011, *Non-Newtonian flow and applied rheology: engineering applications*, Butterworth-Heinemann,

[28] T. Bandyopadhyay, S. Sandhibigraha, S. K. Das, Experimental and CFD analysis of non-Newtonian pseudoplastic liquid flow through vertical helical coil, *American Journal of fluid dynamics*, pp. 56-68, 2014.

[29] A. Metzner, J. Reed, Flow of non-newtonian fluids—correlation of the laminar, transition, and turbulent-flow regions, *Aiche journal*, Vol. 1, No. 4, pp. 434-440, 1955.

[30] J. Yin, C. Teodosiu, Constrained mesh optimization on boundary, *Engineering with Computers*, Vol. 24, No. 3, pp. 231-240, 2008.

[31] W. Jeong, J. Seong, Comparison of effects on technical variances of computational fluid dynamics (CFD) software based on finite element and finite volume methods, *International Journal of Mechanical Sciences*, Vol. 78, pp. 19-26, 2014.

[32] A. Katz, V. Sankaran, Mesh quality effects on the accuracy of CFD solutions on unstructured meshes, *Journal of Computational Physics*, Vol. 230, No. 20, pp. 7670-7686, 2011.

[33] F. Afshari, H. G. Zavaragh, B. Sahin, R. C. Grifoni, F. Corvaro, B. Marchetti, F. Polonara, On numerical methods; optimization of CFD solution to evaluate fluid flow around a sample object at low Re numbers, *Mathematics and Computers in Simulation*, Vol. 152, pp. 51-68, 2018.

[34] J. L. Thomas, B. Diskin, C. L. Rumsey, Towards verification of unstructured-grid solvers, *AIAA journal*, Vol. 46, No. 12, pp. 3070-3079, 2008.

[35] M. C. Ramos, A. L. Costa, V. V. A. Silva, C. P. B. Lima, M. A. F. Veloso, Numerical simulation and validation of laminar flow through a 2D pipe using computational fluid dynamics, *Brazilian Journal of Development*, Vol. 9, No. 10, pp. 28793-28807, 2023.

[36] R. Yin, W. Chow, Comparison of four algorithms for solving pressure-velocity linked equations in simulating atrium fire, *International Journal on Architectural Science*, Vol. 4, No. 1, pp. 24-35, 2003.

[37] I. Dzijan, Z. Virag, S. Krizmanic, COMPARISON OF THE SIMPLER AND THE SIMPLE ALGORITHM FOR SOLVING THE NAVIER-STOKES EQUATIONS ON A COLLOCATED GRID, *Transactions of FAMENA*, Vol. 30, No. 1, pp. 27-36, 2006.